VPS VIBRATIONS IN PHYSICAL SYSTEMS

DOI: 10.21008/j.0860-6897.2021.2.03
Vibrations in Physical Systems, 32(2):2021203, 2023

The Impact of the Sound Reflection Model on the Ray Tracing Simulation Variability

Wojciech BINEK[1], Aleksandra CHOJAK[1], Tadeusz KAMISIŃSKI[1]

Corresponding author: Wojciech BINEK, email: wbinek@agh.edu.pl

[1] AGH University of Science and Technology, Mickiewicza Av. 30, 30-059 Cracow, Poland

Abstract Geometrical acoustics is the most commonly used method of room acoustics prediction. Its efficiency can be improved by explicit calculation of ray contribution to each receiver during reflection called algebraic reflection. The aim of this research is to analyse the applicability and impact of reflection model choice on algebraic reflection calculation using the ray tracing with next event estimation. The tested reflection models include the specular and Lambert reflection combination and the Phong reflection model. Classical ray tracing algorithm, without algebraic reflections, is used as a reference. Based on simulation results and statistical analysis we conclude that the change of the reflection model significantly affects the acoustics conditions within the simulation changing echograms in early reflections region and the reverberation times. Statistical analysis proved that echograms obtained with the combination of ray tracing with next event estimation and Phong reflection model have lowest simulation to simulation variability.

Keywords: geometrical acoustics, BRDF, diffuse rain, next event estimation

1. Introduction

Geometrical acoustics is the most commonly used method of room acoustics prediction. The acoustic rendering equation formalized by Siltanen et al. [1] provides a mathematical framework for the description of a wide variety of geometrical acoustics methods [2,3]. The acoustics rendering equation introduces an acoustic bidirectional reflectance distribution function (BRDF) to describe the reflective properties of the surface. The most common reflection model combines ideally specular and perfectly diffuse reflection. The ratio between the two is defined by the scattering coefficient [4]. In our previous work we presented an alternative reflection model – a measurement-fitted Phong reflection model [5].

Ray tracing efficiency, especially for early reflections, can be improved by explicit calculation of ray contribution to each receiver during each reflection. Such an approach is called algebraic reflection [6] and is used in several algorithms such as ray tracing with next event estimation [7, 8] or diffuse rain algorithm [9]. Unfortunately, the choice of reflection model can affect the ability to calculate reflection at the receiver. For the classical combination of ideally specular and Lambertian reflection only the diffuse part can be explicitly calculated. To overcome this limitation a reflection model with specular reflection described by the non-delta function must be used. Such an approach was presented by Molin et al. [6], where the specular part of the reflection was simulated as a cone with a constant apex angle; however, this is a significant simplification of the reflection as the size of the specular cone may vary [10].

The aim of this research is to analyse the applicability and impact of reflection model choice on algebraic reflection calculation using the ray tracing with next event estimation. The tested reflection models include the specular and Lambert reflection combination and the Phong reflection model. Classical ray tracing algorithm, without algebraic reflections, is used as a reference.

2. Sound reflection modelling

The room acoustics rendering equation [1] introduced the concept of bidirectional reflectance distribution function (BRDF) to describe the reflective properties of a surface. In general, the BRDF is a function of incoming and outgoing directions Θ_i, Θ_o respectively describing the ratio of energy reflected in direction Θ_o for the incidence direction Θ_i.

2.1. Basic reflection model

The classical reflection model combining ideally specular reflection with Lambert diffusion at point x' can be defined in compliance with BRDF definition as:

$$f(x', \Theta_i, \Theta_o, \alpha, s) = (1-s)(1-\alpha)\frac{\delta(\Theta_s - \Theta_o)}{|\Theta_o \cdot N_x|} + s(1-\alpha)\frac{1}{\pi}, \tag{1}$$

where Θ_s is specular reflection direction, δ is the Dirac delta function and $|\Theta_o \cdot N_x|$ is the absolute value of the cosine between the outgoing direction and the surface normal. The classical model depends on material absorption coefficient α and scattering coefficient s which are typically provided by the user. Using the classical model for a given angle of incidence there is only one outgoing direction Θ_o, where specularly reflected part is nonzero. As a result, the algebraic reflection can be effectively calculated only for the diffuse part of the reflection.

2.2. Phong reflection model

The Phong reflection model in acoustics can be defined as:

$$f(x', \Theta_i, \Theta_o, \alpha, s) = (1-s)(1-\alpha)\frac{1}{\rho(x, \Theta_i, n)}\,|\Theta_s \cdot \Theta_o|^n + s(1-\alpha)\frac{1}{\pi}, \tag{2}$$

where $|\Theta_s \cdot \Theta_o|^n$ is the absolute value of the cosine of the angle between specular reflection direction and the observation directions raised to the nth power and $\rho(x, \Theta_i, n)$ is a normalization factor. The normalization factor can be calculated according to the recursive formula provided by Arvo [11].

The Phong reflection model introduces a new parameter n describing the width of the specular reflection cone (Fig. 1). As the n factor increases, the specular reflection becomes narrower. In our previous works, we presented that the model can be fitted to measured reflection patterns [5] and that the n exponent factor can be derived from scattering or diffusion coefficient [10].

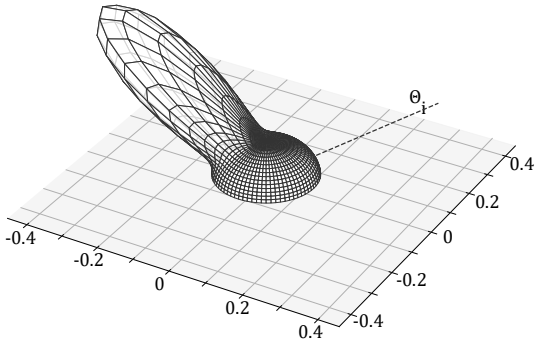

Fig. 1. 3D visualization of normalized Phong reflection model with incidence direction marked (dashed line), radius from point [0,0] represents the energy reflected in given direction, scattering coefficient 0.8, n exponent 20, incidence angle Θ_i 45°.

A significant advantage of the Phong reflection model for ray tracing is the ability to explicitly calculate the specular reflection contribution to each receiver as the specular part of the reflection is non-zero for most of the directions (in the worst case scenario, for 90° incidence angle, the non-zero specular part is a quarter of a hemisphere).

3. Ray tracing with next event estimation

The next event estimation algorithm can be used with various geometrical simulation methods. It introduces an algebraic reflection [6] (also known as *shadow ray*) added to the receiver at each reflection point (Fig. 2). The algorithm was initially developed for computer graphics [7] and then adopted with modifications for acoustics [6, 8, 9]. The reflection contribution at a receiver is calculated explicitly without randomization. In actual implementation, the shadow ray energy can be directly added to the receiver without actual ray casting. The principal idea of the next event estimation is the same as in ray tracing with diffuse rain [9], however, its general implementation is not limited to diffuse reflections only.

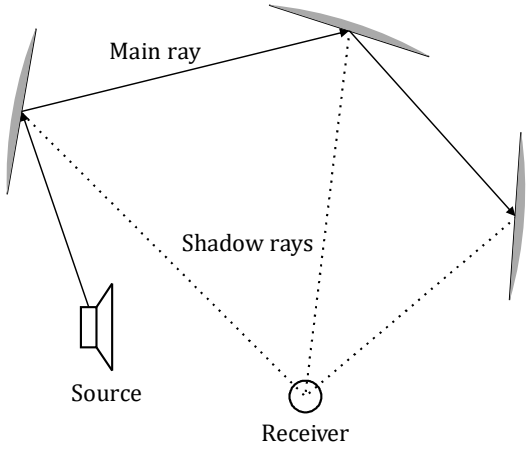

Fig. 2. Schematic representation of ray tracing with next event estimation. For each reflection an algebraic *shadow ray* contribution is added to the receiver.

The shadow ray contribution from the reflection point x'_{ref}, with face normal N_{ref} to a receiver subtending a solid angle Ω_{rec} can be calculated using the following formula (derived from [1, 7]):

$$\Phi_{rec} = L(x'_{ref}, \Theta_i) \int_{\Omega_{rec}} f(x'_{ref}, \Theta_i, \Theta_{ref\to rec}, \alpha, s) \left|\Theta_{ref\to rec} \cdot N_{ref}\right| V(x'_{rec}, x'_{ref}) d\omega_{rec} , \tag{3}$$

where the $V(x'_{rec}, x'_{ref})$ is a visibility term which is 1 if the corresponding part of the receiver is visible and 0 if there is an obstacle between the reflection point and the receiver. The $\left|\Theta_{ref\to rec} \cdot N_{ref}\right|$ factor is the absolute value of the cosine between the observation angle and a face normal. Note that the integration in Eq. (3) is done over the solid angle subtended by the receiver, not the receiver surface itself.

Exact analytical calculation of the integral from Eq. (3) for a surface or a volumetric receiver is usually impossible therefore some simplifications are made. We assume is that the cosine weighted BRDF is constant for all the solid angle Ω_{rec} and we do not consider partial visibility. Using the abovementioned simplifications, for a surface receiver with an area A_r, facing the reflection point, located at a distance $\left\|x'_{rec} - x'_{ref}\right\|$ from the reflection point, the shadow ray contribution can be calculated using the following formula:

$$\Phi_{rec,surf} = L(x'_{ref}, \Theta_i) f(x'_{ref}, \Theta_i, \Theta_{ref\to rec}, \alpha, s) \left|\Theta_{ref\to rec} \cdot N_{ref}\right| \frac{A_r}{\left\|x'_{rec} - x'_{ref}\right\|^2} V(x'_{rec}, x'_{ref}) \tag{4}$$

where the $A_r/\left\|x'_{rec}-x'_{ref}\right\|^2$ is the solid angle subtended by the receiver projection.

For a volumetric receiver we must include the length of the ray-receiver intersection. The simplest solution is to calculate the cylindrical receiver with base radius r and height $2r$ oriented along ray direction. This can be done by multiplication of the surface receiver result by $2r$. Then to convert the cylindrical receiver to a spherical receiver we have to compensate for additional volume, which can be done by multiplying the result by $2/3$ (ratio of sphere volume to cylinder volume). Finally, the equation for spherical receiver contribution is:

$$\Phi_{rec,sph}=L\left(x'_{ref},\Theta_i\right)f\left(x'_{ref},\Theta_i,\Theta_{ref\to rec},\alpha,s\right)\left|\Theta_{ref\to rec}\cdot N_{ref}\right|\frac{0.667A_r\,r}{\left\|x'_{rec}-x'_{ref}\right\|^2}V\left(x'_{rec},x'_{ref}\right). \tag{5}$$

It is worth noting that explicit ray calculation is usually exact for punctual receivers and simplified for surface or volumetric receivers, which is opposite to typical ray tracing, where a volumetric receiver is required to gather a sufficient number of rays.

To calculate the visibility term, we performed ray casting to find the nearest intersection of shadow ray with the model. If the distance from the reflection point to the next model intersection was larger than the distance to the receiver we assumed full visibility, otherwise we assumed no visibility. Although it is a significant simplification, due to large number of rays in simulation the actual error should be relatively small.

4. Methodology

To evaluate the proposed method we used a theatre model with a volume of 4000 m^3 and a capacity of 540 people. The average measured reverberation time inside the room is 1.28 s. Simulations were made for 2 source positions and 20 point receivers (Fig. 3). Four receivers were placed on the stage and remaining 16 were on the ground floor audience, receivers R17-20 were placed under the balcony.

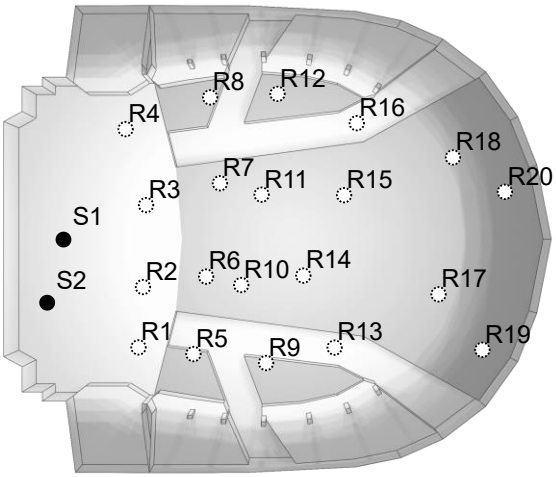

Fig. 3. View of the ground floor of the theatre model with sources (S1-2) and receivers (R1-20) positions marked, shadow shows the approximate contour of the balcony.

Simulations were carried using a classical ray tracing algorithm (RT) and ray tracing with next event (RTNEE) estimation for both specular-Lambert (SL) reflection model and for Phong model. Each simulation was carried 50 times to evaluate the statistical properties of the obtained results. Simulations were made with 500 000 rays for classical RT algorithm and 50 000 rays for RT-NEE to obtain comparable simulation times for each scenario.

To measure the variability of the simulations, for each source-receiver-frequency combination we calculated the average SPL ($\widehat{SPL_t}$, calculated using energetic summation) of each echogram timestep t within the $N=50$ simulation repetitions and a mean absolute error (MAE) between the average SPL and the value from each repetition (Eq. 6).

$$MAE_t = \sum_{i=1}^{N} \frac{\left| SPL_{n,t} - \widehat{SPL_t} \right|}{N}. \tag{6}$$

Higher MAE values indicate higher simulation to simulation variability of the echograms. As a single digit measure, we calculated the median of MAE for each scenario. To test if the change of MAE between different scenarios is statistically significant, we used Kruskal-Wallis test for distributions equality. The analysis of variance (ANOVA) could not be used as the MAE distributions failed the normality tests. To establish which of the results differ from each other, we used Conover's post-hoc test.

Additionally, we compared the reverberation times T20 in the octave bands averaged for all source-receiver combinations to test if the change of the reflection model or the ray tracing algorithm affects the simulated acoustical parameters of the room. To check the statistical significance of mean reverberation time change for each frequency band we used Kruskal-Wallis test performed on set of reverberation times obtained from 50 simulation repetitions followed by Conover post-hoc test.

5. Simulation results

Individual results are presented for source S1, receiver R10 and frequency 1000 Hz. The beforementioned combination was selected randomly, however it is representative for most of the source-receiver-frequency combinations as proved by statistical analysis.

Visual inspection of calculated echograms proves that MAE for RT algorithm is comparable for SL reflection model and Phong reflection model (Fig. 4). However, a change of echogram curve shape can be observed for early reflections. Such behaviour can be expected as changing the reflection model effectively changes the acoustic properties of the model. For ray tracing with next event estimation and SL reflection the number of rays for RTNEE is smaller than for classical RT algorithm (to maintain comparable simulation times), therefore the number of specular reflections hitting the receiver decreases while increasing the energy carried by individual rays. This leads to the existence of significant peaks in the echograms. For SL reflection model this effect cannot be compensated by the algebraic reflection calculation, as it cannot be performed for ideally specular reflection. This problem is solved when using the RTNEE algorithm with Phong reflection model. The echograms have the lowest MAE equal to 0.91 dB as compared to 2.4 dB for RTNEE with SL reflection and slightly less than 6 dB for both classical RT simulations (Fig. 4). No additional peaks are observed, however similarly to the results from classical RT with Phong reflection the shape of the echogram curve differs from the results obtained using SL reflection, especially in the first reflections region.

Tab. 1. Comparison of selected averaged simulation parameters for different simulation algorithms and reflection models.

Simulation scenario	MAE median (averaged for all source-receiver-frequency) combinations	T20, 125 Hz (averaged for all source-receiver combinations and simulation repetitions)	T20, 1000 Hz (averaged for all source-receiver combinations and simulation repetitions)
RT, SL	6.60 dB	1.35 s	1.25 s
RT, Phong	6.47 dB	1.30 s	1.25 s
RTNEE, SL	3.44 dB	1.34 s	1.26 s
RTNEE, Phong	1.47 dB	1.29 s	1.25 s

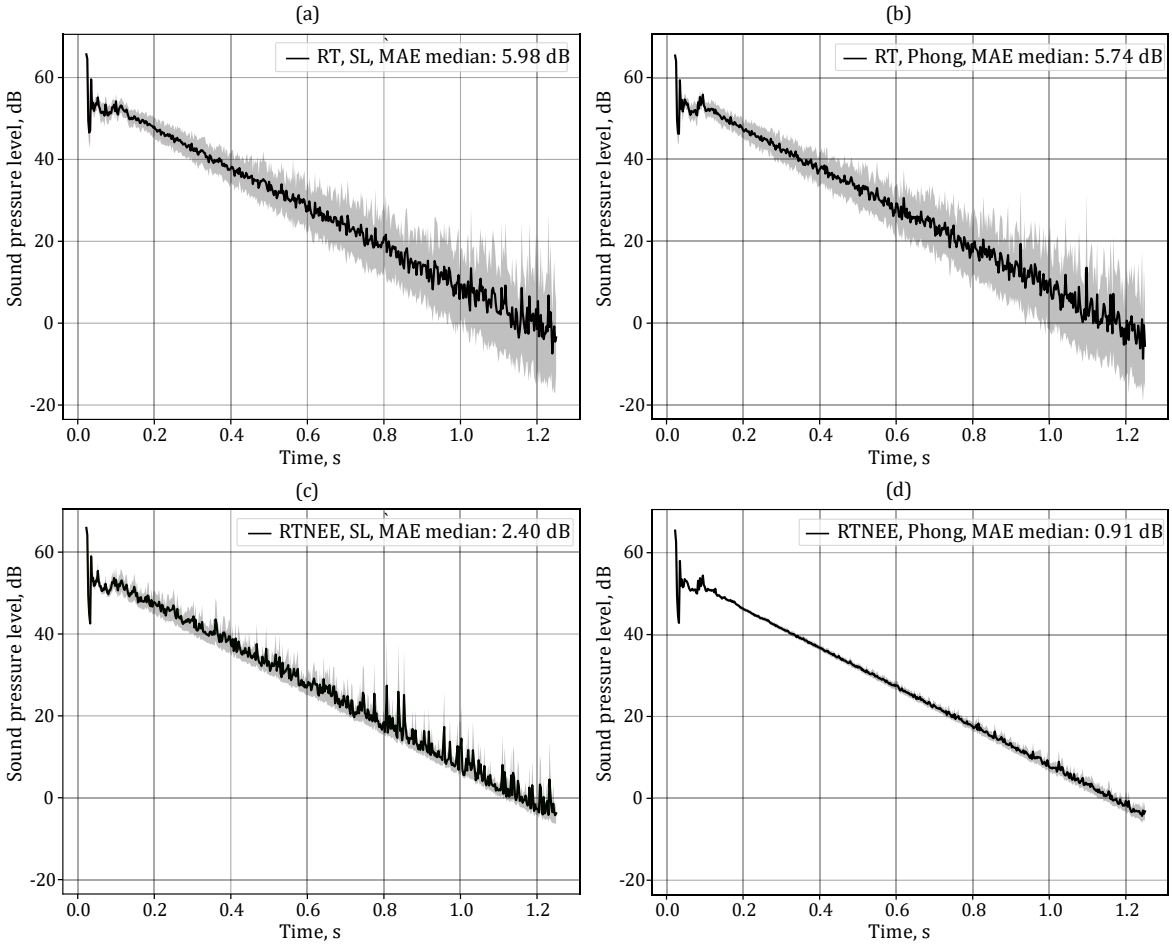

Fig. 4. Comparison of echograms with MAE (marked as grey areas) and MAE median, source S1, receiver R10, frequency 1000 Hz, (a) results of ray tracing (RT) and SL reflection model, (b) results of ray tracing (RT) and Phong reflection model, (c) results of ray tracing with next event estimation (RTNEE) and SL reflection model, (d) results of ray tracing with next event estimation (RTNEE) and Phong reflection model.

Shapiro-Wilk test showed that the MAE distributions are not normal, therefore to test the statistical significance of MAE change, with the change of simulation parameters and reflection models, a Kruskal-Wallis test was used. The Kruskal-Wallis test proved that the MAE distributions are significantly different between the four test cases for all 240 source-receiver-frequency combinations. Post-hoc analysis using Conover test showed that for all cases MAE distributions are equal for classical RT algorithm when comparing between both reflection models. It also proved MAE differences to be significant between the results obtained using the RT and RTNEE for Phong model in all cases and for SL model in 225 of 240 cases. The 15 outliners were the results from receivers R1-4, located on the stage and frequencies 125 Hz, 250 Hz, for which the diffusion coefficients in the model are the lowest. Results obtained with RTNEE and Phong or SL model were significantly different in all cases. MAE median, averaged for all source-receiver-frequency combinations (Tab. 1), equals: for RT with SL 6.60 dB, for RT with Phong 6.47, for RTNEE with SL 3.44 dB, for RTNEE with Phong 1.47 dB, meaning that combination of RTNEE with Phong reflection model has the lowest echogram variability.

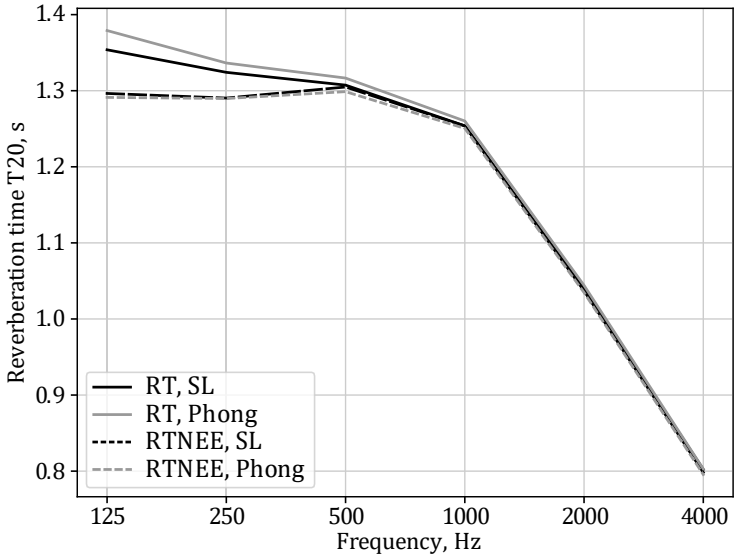

Fig. 5. Comparison of reverberation times between different simulation algorithms and reflection models.

The change of the reflection model significantly affects the average reverberation times changes for 125 Hz and 250 Hz bands (Fig. 5). The changes were proven to be statistically significant. Differences between SL and Phong models are expected as changing the reflection model changes the acoustic properties of the simulated interior. The disparities are caused by smaller diffusion coefficients in low frequency range compared to other frequency bands leading to higher differences between SL and Phong BRDFs. To obtain the same acoustics parameters the reflection model change should be followed by model tuning. The reverberation time changes also for RTNEE with SL reflection, as the peaks observed in the echograms can affect the reverberation time calculations. For higher frequencies although the differences between the reverberation times are statistically significant, they are equal or lower than 0.01 s (Tab. 1) what makes them neglectable in practical applications.

6. Conclusions

We presented the analysis of the impact of reflection model choice on ray tracing simulation results with and without algebraic reflections. The reflection models were compared in classical ray tracing and ray tracing with next event estimation. We described the basic mathematical equations for ray tracing with next event estimation as well as the analysed reflection models.

Based on simulation results and statistical analysis we conclude that the change of the reflection model significantly affects the acoustics conditions within the simulation changing echograms in early reflections region and the reverberation times. To maintain the same acoustic parameters, change of the reflection model should be followed by model tuning. Statistical analysis proved that echograms obtained with the combination of ray tracing with next event estimation and Phong reflection model have lowest simulation to simulation variability. This proves the applicability of Phong model in algebraic reflection calculations. The combination of specular and Lambert reflection model should be used in algebraic reflections algorithms with caution as it may create additional peaks in the echograms, if we reduce the initial number of rays to maintain simulation time as for classical ray tracing. Therefore, its usefulness for algebraic reflection calculation is questionable.

Additional information

The authors declare no competing financial interests.

References

1. S. Siltanen, T. Lokki, S. Kiminki, L. Savioja. The room acoustic rendering equation. J. Acoust. Soc. Am., 122(3):1624–1635, 2007. DOI: 10.1121/1.2766781
2. S. Laine, S. Siltanen, T. Lokki, L. Savioja. Accelerated beam tracing algorithm. Appl. Acoust. ,70: 172–181, 2009. DOI: 10.1016/j.apacoust.2007.11.011
3. L. Savioja, U. P. Svensson. Overview of geometrical room acoustic modeling techniques. J. Acoust. Soc. Am., 138(2):708–730, 2015. DOI: 10.1121/1.4926438
4. ISO 17497-1:2004 Acoustics – Sound-scattering properties of surfaces – Part 1: Measurement of the random-incidence scattering coefficient in a reverberation room. 2004.
5. W. Binek, A. Pilch, T. Kamisiński. Application of fitted to measurements sound reflecion model in geometrical acoustics simulations, in INTER-NOISE 2019 MADRID - 48th International Congress and Exhibition on Noise Control Engineering, 2019.
6. E. Molin, D. Bard, J. Negreira. Algebraic reflections in geometric acoustics. Proceedings of Meetings on Acoustics, 30(1):22002, 2017. DOI: 10.1121/2.0000621
7. E. P. Lafortune. Mathematical Models and Monte Carlo Algorithms for Physically Based Rendering, PhD Thesis, Katholieke Universiteit Leuven, 1995.
8. W. Binek. Ray tracing with next event estimation in room acoustics simulations [Metoda promieniowa z estymacją następnego zdarzenia w symulacjach akustyki pomieszczeń], MSc Thesis, Akademia Górniczo-Hutnicza im. Stanisława Staszica w Krakowie, 2016.
9. D. Schröder. Physically based real-time auralization of interactive virtual environments. Logos Verlag, Berlin, 2011.
10. W. Binek, T. Kamisiński. Adaptation and preliminary evaluation of phong reflection model in room acoustic simulations [Adaptacja i wstępna ewaluacja modelu odbicia Phoga w symulacjach akustyki pomieszczeń]. Postępy Akustyki 2017, 401–411.
11. J. Arvo. Applications of Irradiance Tensors to the Simulation of Non-Lambertian Phenomena. Comput. Graph. (SIGGRAPH ’95 Proceedings), 335–342, 1995. DOI: 10.1145/218380.218467